Tellus (1990), *42B*, 389–407

A regional numerical sulfur dispersion model using a meteorological model with explicit treatment of clouds

By ERIK BERGE, *Section of Meteorology, University of Bergen, Allégt. 70, N-5007 Bergen, Norway*

(Manuscript received 15 November 1989; in final form 18 June 1990)

ABSTRACT

A regional numerical short-term (hours to days) sulfur dispersion model, interacting with a NWP-model with a detailed treatment of clouds and condensation, is formulated and tested. The model has 10 layers in the vertical, 50 km horizontal resolution and covers NW-Europe. It is initialized with model-simulated fields of sulfur dioxide and sulfate in air, based on realistic sulfur SO_2 emission fields. A simple parameterization scheme for dry deposition, oxidation, uptake by clouds and deposition by precipitation is applied. The numerical treatment ensures positive-definite and mass-conserving solutions. A comparison between a 36-h integration on a real synoptic situation and surface measurements, suggests that the wet deposition of sulfate and the sulfate in air is underestimated over Scandinavia. SO_2 in air is overestimated close to the sources. The simulations indicate that both the oxidation rate and the vertical transport by eddy diffusion are too low.

1. Introduction

The increasing environmental impacts of man-made emission on the atmosphere, have made a strong need for development of regional air pollution models. Together with pollutant measurements a regional air pollution model coupled to a meteorological model is necessary for the understanding of the transformation, dispersion and removal of pollutants.

This type of coupling has been introduced in regional Lagrangian models for studying the long term (months and years) transport of sulfur and nitrogen compounds in Europe (Eliassen and Saltbones, 1983; Hov et al., 1988). Attempts have also been made to simulate short-term (hours and days) transport by regional Eulerian model. Pudykiewicz et al. (1985) apply dry air sulfur and nitrogen chemistry to a 3-D numerical weather prediction model in North America. Charmichael and Peters (1984a, b) use meteorological fields analysed from observations to simulate 3-D sulfur transport in the lower troposphere over North America. The importance of in-cloud and precipitation processes to pollution transport and removal, has increased the efforts of modelling these processes. Charmichael et al. (1986), Tremblay and Leighton (1986) and Rutledge et al. (1986) utilize simplified meteorological models to study parameterizations of clouds and chemical processes. Chaumarliac et al. (1987) use a 3-D mesoscale meteorological model for 2-D studies of a microphysical and chemical sulfur scavenging scheme. Chang et al. (1987) have formulated a 3-D treatment of different chemical compounds including liquid phase chemistry together with an NWP-model. A comparison between precipitation chemistry data and results from this model is presented in Middleton et al. (1988).

Even though elaborate 3-D chemical and meteorological models exist, the description of cloud/condensation/precipitation processes has so far received little attention and is often treated in a strongly simplified manner (Sundqvist et al., 1989). Consequently the description of the cloud and precipitation dependent chemical processes in these models become quite uncertain. The aim of this paper is to couple a regional sulfur transport model to a 3-D meteorological model, with emphasis on including the wet scavenging of sulfur (the most important component in acid

rain) into a realistic description of clouds and precipitation. Model simulations on a real synoptic situation will be presented and compared to observations of sulfur compounds in dry air and precipitation.

The paper represents a pilot study in including explicit treatment of cloud- and precipitation scavenging of sulfur into the NWP-model at the Section of Meteorology, University of Bergen (AMUB). The AMUB-model is a research version of the Norwegian Meteorological Institute (DNMI) meso scale model. The AMUB-model contains a refined cloud/condensation scheme, with cloud water as a prognostic variable. The inclusion of this scheme indicate an improvement of the model calculations compared to that obtained by the original DNMI-model (Sundqvist et al., 1989; Kristjansson, 1990). The cloud/condensation scheme is the basis for the explicit treatment of the wet scavenging processes.

As a first approach, a simplified representation of the chemical processes described by a bulk transformation rate is selected. Uptake by clouds and deposition by precipitation is also described in a simplified manner. Emphasis is put on a mass conserving and positive definite numerical treatment. In addition to the chemical transformation and wet deposition, other processes (vertical transport, dry deposition, emission and numerical dispersion) of importance to the sulfur model are discussed, and the possible improvements of the model are pointed out. The sulfur model is an online model without any feedback on the meteorlogical model.

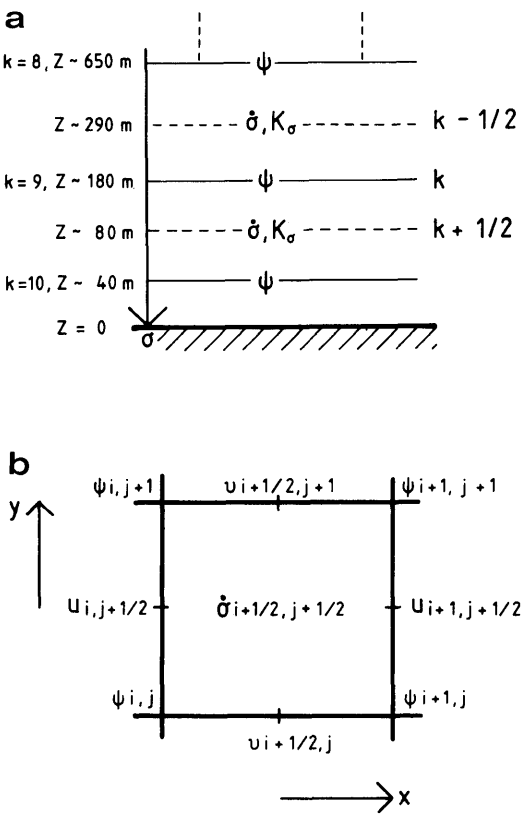

Fig. 1. (a) Vertical arrangement of the model variables and the approximate height (m) of the lowest σ-levels, and (b) horizontal arrangement of the model variables. ψ represents chemical compounds, temperature, moisture or cloud water.

2. The numerical weather prediction model

The numerical weather prediction model (the AMUB-model), which is the basis for the pollution modelling, is based on the operational fine mesh model of the Norwegian Meteorological Institute (DNMI). The numerical design of this model is documented by Grønås et al. (1987). The implementation of physical (non-adiabatic) processes is presented in Nordeng (1987). The AMUB-model is a primitive equations grid point model with sigma, σ, as the vertical coordinate

$$\sigma = \frac{p - p_t}{p^*}, \tag{2.1}$$

where $p^* = p_s - p_t$ and p, p_s and p_t are the pressures at an arbitrary level, at the surface and at the top of the model atmosphere respectively. Here, 10 levels in the vertical and $P_t = 200$ mb are used.

The vertical arrangement of the variables and the approximate heights (in meters) of the lowest σ-levels are given in Fig. 1a. The model variables are horizontally distributed according to the Arakawa D-grid (Mesinger and Arakawa, 1976) shown in Fig. 1b. We employ a horizontal resolution of 50 km on the geographical domain shown in Fig. 2. To maintain stable numerical solutions the maximum time step is 150 s. It is observed from Fig. 1, that the grid is staggered

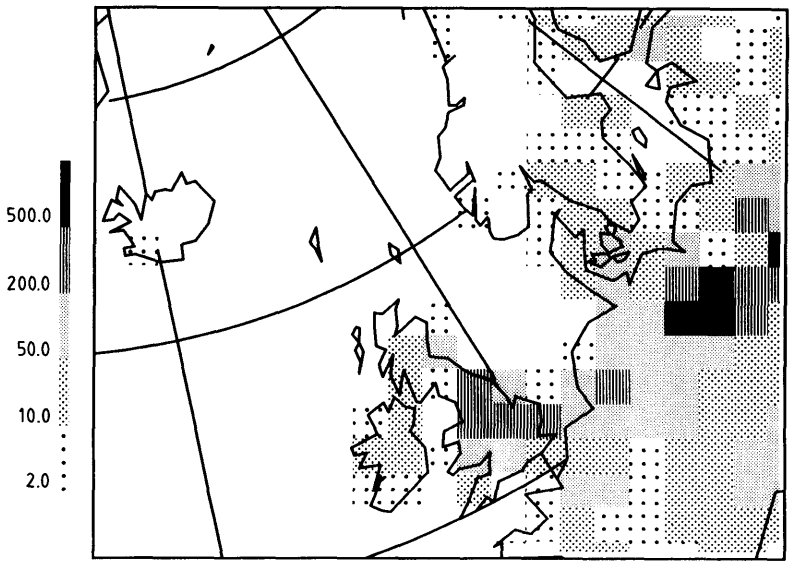

Fig. 2. Geographical view of the model domain, and the sulfur emission (10 tonnes/day) applied to the days 5–6 September 1985.

both in the horizontal and the vertical. The levels at which the vertical velocity, $\dot{\sigma}$, is defined, will be referred to as the half levels.

The cloud/condensation scheme (Sundqvist et al., 1989) parameterizes stratiform and convective condensation and cloud formation. On one hand the scheme parameterizes the microphysical processes which divide the condensate between cloud water and precipitation. On the other hand, since clouds are generally not resolved by the model grid, the scheme also parameterizes the partitioning between cloudy and cloud free parts in each grid box, i.e., a fractional cloud coverage is calculated. The subgrid parameterization is applied only in the horizontal. The clouds fill the whole grid box in the vertical.

To distinguish between convective and stratiform condensation, a test is performed to check whether the grid column in question is conditionally unstable or not. If a parcel of surface air is positively buoyant after being lifted vertically to saturation, convective condensation is considered. If not, the possibility for stratiform condensation to occur is investigated.

In both the stratiform and the convective case the cloud water content is explicitly treated through a prognostic equation.

3. The sulfur-model

The SULFUR-model utilizes the detailed meteorological fields from the AMUB-model to study sulfur transport and formation of acid rain on a short time scale (hours and days). Cloud water content is calculated explicitly, and it is therefore possible to treat the transformation and removal processes of sulfur compounds in clouds explicitly.

The continuity equation is solved numerically for three different sulfur compounds. In the dry phase we consider sulfur dioxide ($S\text{–}SO_2(a)$) and sulfate particles ($S\text{–}SO_4(a)$), and in the liquid phase we consider sulfate in cloud water ($S\text{–}SO_4(cl)$), where a and cl are abbreviations for air and cloud.

If we let ψ represent the mixing ratio (kg-sulfur/kg-air) of one of the sulfur components, the continuity equation can be written

$$\frac{\partial \psi}{\partial t} = -m^2 \nabla_H \cdot (\boldsymbol{V}_H \psi) - \frac{\partial}{\partial \sigma}(\dot{\sigma}\psi) - \frac{\psi}{p^*}\left[\frac{\partial p^*}{\partial t} + m^2 \boldsymbol{V}_H \cdot (\nabla_H p^*)\right] + \left[\frac{g}{p^*}\right]^2 \frac{\partial}{\partial \sigma}\left[\rho^2 (K_z)\frac{\partial \psi}{\partial \sigma}\right] + Q_S + Q_L. \qquad (3.1)$$

The first three terms on the right-hand side represent the flux divergence formulation of the advection equation. V_H and ∇_H are the horizontal wind vector and del operator respectively, and m is the map factor on a polar-stereographic map projection. A scale analysis of these three terms (see Appendix 1) shows that the third term, on an average, is small compared to the two others for the scale of the motions applied to the SULFUR-model. The third term is therefore neglected in the model calculations. The fourth term represents the vertical eddy diffusion, where g, ρ and K_z is the gravitational acceleration, air density and the vertical eddy diffusion coefficient respectively. Horizontal eddy diffusion is not included for any of the three components, and vertical advection and eddy diffusion are omitted for S–SO_4(cl). Q_S and Q_L represent chemical and/or physical source and loss terms. The position of ψ in the numerical grid is shown in Fig. 1a and b.

The parameterization of surface fluxes is based on the Monin–Obukhov similarity theory, while above the surface layer mixing length theory is applied. When stratiform or convective clouds are present, K_z is increased between 1 and 4 times, depending on the current and the saturation lapse rates, and the fractional cloudiness (Sundqvist et al., 1989).

3.1. Emissions

The emission data were obtained from the EMEP (EMEP: Co-operating programme for monitoring and evaluation of the long-range transmission of air pollutants in Europe) inventories through Saltbones (1989, personal communication). The data are given as a mean annual value plus an annual sinusoidal variation, which yields a maximum in January and a minimum in July. The emission field applied in the present simulations, is shown in Fig. 2. The emission rate is considered constant in time during the simulations. Furthermore, the emission data have a resolution of 150 km (i.e., 3×3 grid-boxes).

According to the emission data 64% of SO_2 is released above 100 m, the remainder below (Saltbones, 1989, personal communication). In addition, we anticipate a mean plume rise of about 100 m. Thus we let the emissions take place in layer 9 shown in Fig. 1a. Seinfeld (1975) has reviewed various plume rise estimates, and uncertainties are involved in the present choice. Under certain conditions the effective emission height might be several hundred meters. Uncertainty is also associated with the grid representation of point sources as discussed in Karamchandani and Peters (1983). A detailed method for representing point sources by grid boxes in an urban air pollution is found in McRae et al. (1982). Here it is assumed that the emissions are immediately distributed into a 50-km square horizontally. Since a very strong instantaneous horizontal subgrid diffusion therefore is forced on the emission some instantaneous vertical mixing must be expected as well between the lowest levels in the vertical. No attempt has been made to parameterize this effect. Instead the sensitivity of the sulfur concentration as a function of the initial vertical emission distribution is elucidated in the model runs in Section 5.

In the EMEP-model (Eliassen et al., 1988) 5% of the emission is assumed to be emitted directly as S–SO_4(a). In studies by Prahm et al. (1980) and Rodhe et al. (1981) it was indicated that this percentage might be somewhat higher. Based on the present simulations a percentage of 10 has been found reasonable. The remainder of the emission is S–SO_2(a).

3.2. Dry deposition

A substantial part of the sulfur deposition in northwest Europe (about 50%) comes, in the long term, via dry processes (Rodhe and Granat, 1983). Thus, a realistic description of the dry deposition is important for estimation of sulfur transport. The mechanisms leading to dry deposition of atmospheric constituents are however complicated and still not fully understood (Seinfeld, 1986), and it is beyond the scope of this study to derive a detailed parameterization of these processes.

The dry deposition in atmospheric transport models is usually described by an overall dry deposition velocity, v_D. To obtain the dry deposition flux, F_D, the mixing ratio, ψ_{1m}, at about 1 m above the ground is utilized, which yields

$$F_D = v_D \psi_{1m} \rho. \tag{3.2}$$

The dry deposition velocity is estimated experi-

mentally. Estimates of the SO_2(a) and SO_4(a) deposition velocities are reviewed by Sehmel (1980) and Seinfeld (1986) respectively, and show large variability. The large variability is due to the dependence on the vertical eddy transport near the surface, the surface laminar layer, the absorbing properties of the surface, and uncertainties in the measurements. However, as a first approach, average values are applied to the whole model domain. The values are adopted from the EMEP-model (Eliassen and Saltbones, 1983), and they equal 0.8 cm s^{-1} and 0.2 cm s^{-1} for SO_2(a) and SO_4(a) respectively. The lowest model concentration at level 10, is a mean between the ground and approximately 80 m (Fig. 1b). This value will generally not correspond to the 1 m level concentration needed in (3.2). Specially, when there is small vertical exchange, the concentration at 1 m is expected to be substantially lower than the level 10 value. The concentration applicable to (3.2) is estimated by assuming

$$\psi_{1m} = (C_D/C_0)\psi_{10}, \tag{3.3}$$

where C_D is the actual drag coefficient and C_0 is a reference drag coefficient corresponding to neutral conditions and a surface roughness $Z_0 = 0.3$ m. In the AMUB-model $Z_0 = 0.3$ m over land except for snow, ice and desert where it equals 10^{-3} m. Over sea Z_0 is not allowed to be less than $1.5 \cdot 10^{-5}$, and it seldom becomes above 10^{-3} m. From (3.3) we see that for $Z_0 = 0.3$ m and neutral conditions, it is assumed that the concentration at 1 m equals the level 10 value. The effect of the factor C_D/C_0 is to reduce the 1 m concentration substantially for stable stratification and low wind speeds (Fig. 3). When the wind speed is above 5–10 m s^{-1} there is little effect. For unstable conditions, we use the same formulation as in the neutral case. For reduced surface roughness C_D/C_0 is shifted towards smaller values.

For elevated sources, it is likely that the concentrations increase with height in the constant flux layer. Since eq. (3.3) assumes a uniform concentration at neutral conditions the concentrations applied to eq. (3.2) might be too high, and the dry deposition might become overestimated.

Dry deposition in pollutant transport models has been studied by, for example, Eliassen and

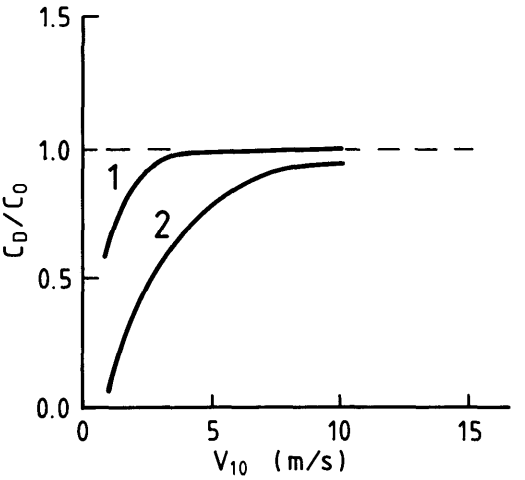

Fig. 3. The ratio C_D/C_0 (defined in the text) as a function of windspeed at σ-level 10, for the surface layer static stabilities (1) $\partial\theta/\partial z = 10^{-3}$°C m^{-1} and (2) $\partial\theta/\partial z = 10^{-2}$°C m^{-1}, and a surface roughness $Z_0 = 0.3$ m.

Saltbones (1983), Isaksen and Rodhe (1978) and McRae et al. (1982). Here we apply the approach given in Isaksen and Rodhe (1978) to compare with the formulation given in eq. (3.3). They calculate the dry deposition velocity (v_{D10}) applicable to the concentration at the lowest model level by

$$v_{D10} = \frac{v_{D1m}}{\left[1 + \frac{v_{D1m}}{C_D|V_{10}|}\right]}, \tag{3.4}$$

where v_{D1m} and V_{10} are the dry deposition velocity 1 m above the surface and the wind at σ-level 10 respectively.

Evidently, some instantaneous subgrid scale dry deposition should also be taken into account in grid squares where emission occurs, and it should to a high degree be governed by the local turbulence. For example, model experiments performed by Nordlund (1986), showed that the local deposition, for cases where the effective emission height is above 100–150 m, may vary from almost zero up to 40% depending on the local stability and wind speed. However, the subgrid scale deposition is so far not included.

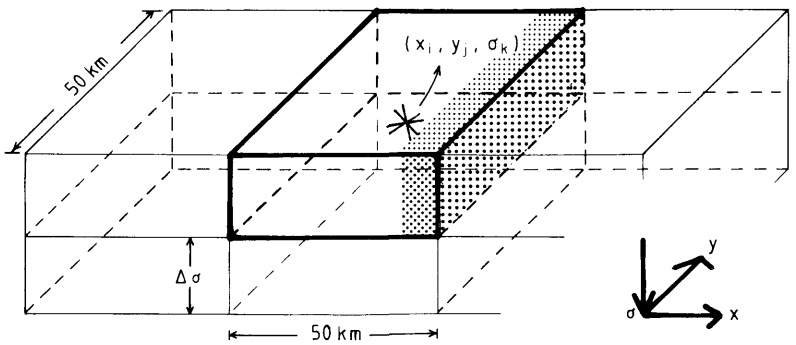

Fig. 4. A grid box with center at (x_i, y_j, σ_k). The shaded area represents the fraction, b, of the box filled with clouds.

3.3. Chemical processes

The transformation of SO_2 to sulfate compounds in the gas phase takes place through the reaction of SO_2 with hydroxyl radicals (OH). The sulfate particles act as cloud condensation nuclei. In the liquid phase, SO_2 is first dissolved into water, then it is oxidized to SO_4, where the two most important oxidizing species are ozone (O_3) and hydrogen peroxide (H_2O_2). The relative importance of the gas and liquid phase sulfate production to the wet deposition of sulfate has been estimated by Fowler (1980). On an average, about 65% of the sulfate originate from condensation nuclei mainly produced by gas phase processes, and about 20% is due to in-cloud processes. The remainder is due to sub-cloud scavenging by raindrops (10%) and brownian diffusion and diffusiophoresis (5%).

However, as a first approach, it has been assumed that all the chemical processes transforming SO_2 to sulfate are simply described by a constant transformation rate, $k_1 = 4 \cdot 10^{-6}$ s^{-1}. This rate corresponds to values used in the EMEP-model (Eliassen and Saltbones, 1983; Eliassen et al., 1988). The expression for the transformation is:

$$\frac{\partial(\text{S–SO}_2\text{(a)})}{\partial t} = -k_1(\text{S–SO}_2\text{(a)}), \tag{3.5}$$

and $\partial(\text{S–SO}_4\text{(a)})/\partial t = -\partial(\text{S–SO}_2\text{(a)})/\partial t$. All the oxidized S–$SO_2$(a) is considered to take the form S–SO_4(a). The uptake of S–SO_4(a) in the clouds takes place during condensation (see next paragraph).

3.4. Wet deposition

Condensation may occur in a fraction, b, of a grid box (see Fig. 4). Consequently, some fraction of the total S–SO_4(a) in the grid box, should be incorporated into the condensate. This fraction is assumed to be equal to b, i.e., we assume that all the S–SO_4(a) in a volume occupied by clouds, is taken up by the clouds. The source/sink term for S–SO_4(cl) becomes

$$\frac{\partial(\text{S–SO}_4\text{(cl)})}{\partial t} = \tfrac{1}{2}[k_2 + |k_2|](\text{S–SO}_4\text{(a)}) + \tfrac{1}{2}[k_2 - |k_2|](\text{S–SO}_4\text{(cl)}), \tag{3.6}$$

where $k_2 = \partial b/\partial t$. The corresponding source/sink term for S–SO_4(a) has opposite sign. No direct uptake of SO_2 in clouds is considered.

In addition, evaporation of cloud water is allowed to take place when cloud water is advected into a grid box where no condensation is occurring. In such cases all the advected cloud water is assumed to evaporate instantly, and hence all the corresponding S–SO_4(cl) is returned back to S–SO_4(a).

The release of precipitation is a function of the local cloud water content. In addition both the coalescence process and the coexistens of water- and ice droplets affect the release of precipitation (Sundqvist et al., 1989). The fractional loss of sulfate in cloud water per unit time due to precipitation has been assumed equal to the fractional release of cloud water per unit time. If we let m_C denote the local cloud water content, $\partial m_P/\partial t$ the local production rate of precipitation,

and hence $k_3 = 1/m_C(\partial m_P/\partial t)$, then the sink term for S–SO_4(cl) due to precipitation becomes

$$\frac{\partial(\text{S–SO}_4(\text{cl}))}{\partial t} = -k_3(\text{S–SO}_4(\text{cl})). \tag{3.7}$$

The resulting accumulated wet deposition per unit time and unit area, A_S, at the ground is given by

$$A_S = \frac{p_s - p_t}{g} \int_{\sigma_T}^{\sigma_B} [k_3(\text{S–SO}_4(\text{cl}))]\, d\sigma, \tag{3.8}$$

where σ_B and σ_T are the bottom and the top of the clouds respectively.

Sub-cloud scavenging might give substantial sulfate contributions, specially close to the sources where the low level concentrations are high. However, on an average this process is not believed to contribute with more than about 10% of the wet deposition of sulfur (Fowler, 1980), and it is so far neglected.

The cloud/condensation scheme also accounts for evaporation of raindrops which increases the sulfur concentration in the rain. During a 36-h simulation about 25% of the released precipitation mass evaporates before reaching the surface. Some small fraction of this mass should be considered as rain drops which evaporate completely, and the corresponding sulfate should be returned to the dry phase. This effect is not yet included, and it means that small amounts of sulfur might be deposited through (3.7), even though no rain is falling.

4. Numerical solution techniques

When the continuity eq. (3.1) is solved numerically, we require the solution to be mass conserving and positive. Negative values of a pollutant are not physically realistic.

We rewrite eq. (3.1) using the notation ψ_1, ψ_2 and ψ_3 for S–SO_2(a), S–SO_4(a) and S–SO_4(cl) respectively, to

$$\frac{\partial \psi_n}{\partial t} = (A_1 + A_2)\psi_n + \sum_{m=1}^{3} (A_3^{nm} + A_4^{nm} + A_5^{nm})\psi_m,$$

$$n = 1, 2, 3, \tag{4.1}$$

where

$$A_1 = \left[\frac{g}{p^*}\right]^2 \frac{\partial}{\partial \sigma}\left[\rho^2(K_z)\frac{\partial}{\partial \sigma}\right],$$

$$A_2 = -m^2\left[\nabla_H\cdot(V_H) - \frac{1}{m^2}\frac{\partial}{\partial \sigma}(\dot{\sigma})\right],$$

$$A_3 = \begin{bmatrix} -k_1 & 0 & 0 \\ k_1 & 0 & 0 \\ 0 & 0 & 0 \end{bmatrix},$$

$$A_4 = \begin{bmatrix} 0 & 0 & 0 \\ 0 & -\frac{1}{2}(k_2 + |k_2|) & -\frac{1}{2}(k_2 - |k_2|) \\ 0 & \frac{1}{2}(k_2 + |k_2|) & \frac{1}{2}(k_2 - |k_2|) \end{bmatrix},$$

$$A_5 = \begin{bmatrix} 0 & 0 & 0 \\ 0 & 0 & 0 \\ 0 & 0 & k_3 \end{bmatrix}.$$

Vertical advection and eddy diffusion are neglected for S–SO_4(cl), the dry deposition and emission of S–SO_2(a) and S–SO_4(a) are incorporated in the eddy diffusion terms, and when evaporation occurs all S–SO_4(cl) is transformed back to S–SO_4(a). The operators $A_1, \ldots, A_5$ represent diffusion, advection, dry phase processes, cloud processes and wet deposition, respectively.

One simple approach to the time discretization of (4.1), is to assume each operator on the right-hand side of the equation independent during a timestep Δt. After calculating the corresponding numerical tendencies, these are simply added together at the end of the time step. Hence

$$\psi_n^{\tau+1} = \psi_n^{\tau} + \Delta t\left[(A_1 + A_2)\psi_n + \sum_{m=1}^{3} (A_3^{nm} + A_4^{nm} + A_5^{nm})\psi_m\right], \quad n = 1, 2, 3, \tag{4.2}$$

where Δt and τ are the time increment and the timestep index. However, when this method was applied, the term in square brackets in eq. (4.2) became in some cases negative with an absolute value greater than ψ^{τ}. Thus the result was a negative $\psi^{\tau+1}$. This occurred for S–SO_4(cl) when there was a loss due to both precipitation and reduction of the grid box cloudiness at the same time. Principally this is a consequence of a time extrapolation over too long a time step. The square bracket term has to be allowed to adjust to new ψ-values over shorter intervals.

To avoid this problem the time discretization of eq. (4.1) is instead performed with the fractional step method (see Richtmyer and

Morton, 1967; McRae et al., 1982). The method consists of successively applying the operators $A_1, \ldots, A_5$ by intermediate time integrations.

In many applications, the operators are used to represent different spatial directions, i.e., a complicated three-dimensional problem can be solved by splitting it up into simpler one-dimensional problems. However, the choice of operator splitting is somewhat arbitrary, and in the present model the operators are selected on the basis of physical and chemical processes according to eq. (4.1).

If we assume each intermediate time integration to be positive, the final $\psi^{\tau+1}$ value becomes positive as well. Another advantage of the scheme is the little need for computer storage since the tendencies are not stored.

The time-truncation error in the splitting scheme is of first order; however, if the order of applying the operators is reversed every time step, the scheme becomes accurate to second order (McRae et al., 1982). Applying either the first order or the second order version does not give any significant differences in the results presented in Section 5. In the following a description of the numerical algorithm of each substep is given.

4.1. *Numerical algorithm of each substep*

The vertical diffusion is treated by an implicit method. The advantage of such a method is that it is unconditionally stable numerically. Chemical reactions and wet depositions are represented by constant transformation rates. The solutions are given by a simple explicit time integration.

One of the most important numerical problems in an Eulerian transport model is the numerical dispersion connected with the treatment of the advection term. Rood (1987) reviews advantages and disadvantages of a number of the most common numerical schemes applied to the advection equation. Here, the advection term is treated by a first order upstream scheme. The numerical form of A_2 in eq. (4.1), considering only the advective fluxes in the x-direction becomes (i is the index for the gridpoints in the x-direction)

$$\frac{\psi_i^{\tau+1}-\psi_i^{\tau}}{\Delta t} = -m^2[F_a(\psi_i^{\tau}, \psi_{i+1}^{\tau}, \overline{u}_{i+\frac{1}{2}}^{\tau}) - F_a(\psi_{i-1}^{\tau}, \psi_i^{\tau}, \overline{u}_{i-\frac{1}{2}}^{\tau})], \quad (4.3)$$

where

$$F_a(\psi_i, \psi_{i+1}, \overline{u}_{i+\frac{1}{2}}) = \frac{1}{2\Delta x}[(\overline{u}_{i+\frac{1}{2}} + |\overline{u}_{i+\frac{1}{2}}|)\psi_i + (\overline{u}_{i+\frac{1}{2}} - |\overline{u}_{i+\frac{1}{2}}|)\psi_{i+1}],$$

and $\overline{u}_{i+\frac{1}{2}}$ is the four point mean needed to find a u-value between ψ_i and ψ_{i+1} (see Fig. 1b). The advective fluxes in the y- and σ-direction are obtained in the same way. At the upper and lower boundary the vertical fluxes $F_{a_{k-1/2}}$ and $F_{a_{k+1/2}}$ respectively, are put equal to zero. At the lateral boundaries, the mixing ratios have been put equal to zero.

The main advantage of the upstream scheme is its simplicity and low computational cost. In addition, the scheme is positive definite and mass conserving, but it suffers from strong numerical diffusion that will smooth out spatial gradients. To investigate the effect of a less diffusive scheme on the model simulations, we apply the more complicated "antidiffusion scheme" (suggested by Smolarkiewicz, 1983, 1984) to the horizontal advection. The scheme can be applied with several corrective step and with multiplying the "antidiffusion velocities" with a factor between 1 and 2 in two dimensions. In the present model, we utilize one corrective step and put the factor equal to unity. A discussion of the antidiffusion scheme and two other shape preserving schemes is found in Berge (1988).

4.1.1. Discussion of numerical and physical diffusion. Brost et al. (1988) have investigated numerical and physical diffusion on tracer puffs simulated by regional Eulerian models. They found that the antidiffusion scheme considerably overpredicted the plume size due to numerical diffusion. Since the upstream scheme is even more diffusive it is likely that the inclusion of physical horizontal diffusion in the present model is not useful unless the numerical scheme is substantially improved. This can also be seen by expressing the numerical diffusion coefficient in the upstream scheme by $K_{\text{num}} = 0.5(|u|\,\Delta x - u^2\,\Delta t)$ (Smolarkiewicz, 1983). Since the term $u^2\,\Delta t$ is much smaller than $|u|\,\Delta x$ with the time ($\Delta t = 150$ s) and spatial ($\Delta x = 50$ km) resolution of the model we can write $K_{\text{num}} = 0.5|u|\,\Delta x$. Assuming that the physical diffusion can be

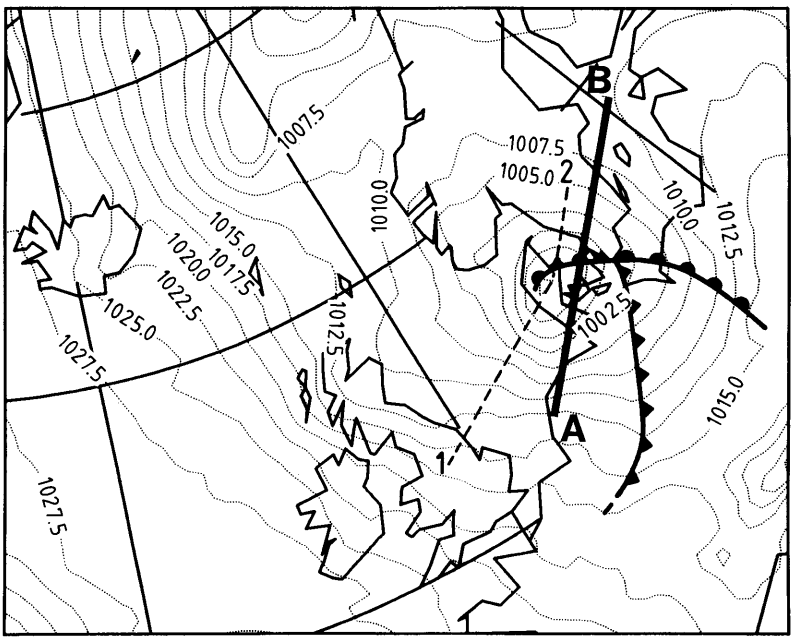

Fig. 5. Position of low at initial time 00Z 5 September (1) and after 36-h integration (2), and mean sea level pressure (mb) after 18 h integration. The position of the warm- and cold front after 18 h, is indicated.

described by mixing length theory, and that the maximum mixing length equals the horizontal grid distance, the maximum horizontal diffusion coefficient would become $K_{max} = \Delta x \Delta u$. Assuming that $\Delta u/u \leqslant 1$, yields $K_{max}/K_{num} \leqslant 2$. This indicates that, for the present model resolution, the numerical diffusion must be expected as large as the physical diffusion, and in some cases probably larger.

In the vertical, the numerical diffusion is often much smaller than the physical diffusion, and the problem is less pronounced. Typical modelled maximum vertical velocities are 10^{-3} m/s close to the ground and 10^{-1} m/s in the free atmosphere. The corresponding vertical resolutions are about 200 m and 1000 m, which yields a maximum K_{num} of 0.1 m^2/s and 50 m^2/s respectively. Thus close to the surface where the main vertical sulfur transport takes place, the effect of the numerical diffusion is small. At the same time the vertical eddy diffusion is important since the vertical advection velocities are small. However, in the middle troposphere the numerical diffusion can be strong, and in some cases greater than the physical diffusion.

5. An example of model performance

In this section, the results of 36 h simulations of sulfur transport, and the significance of the model assumptions will be discussed.

5.1. Description of the weather situation

First of all, we have to select a weather situation which has been successfully simulated by the AMUB-model, otherwise we should not expect the SULFUR-model to give realistic results. The selected case is the same as documented in Sundqvist et al. (1989), and it simulates a storm that forms over southern England and moves northeastward to southern Scandinavia during the 5 and 6 September 1985. The pressure field and fronts after 18 h prognosis and the position of the low for three different times, are shown in Fig. 5. The AMUB-model successfully reproduced the wind-, pressure-, cloud- and precipitation fields for this case. Heavy stratiform precipitation over southern Scandinavia gave large amounts of wet deposition of sulfur during the simulations period. In the beginning of the simulation, a stable planetary boundary layer

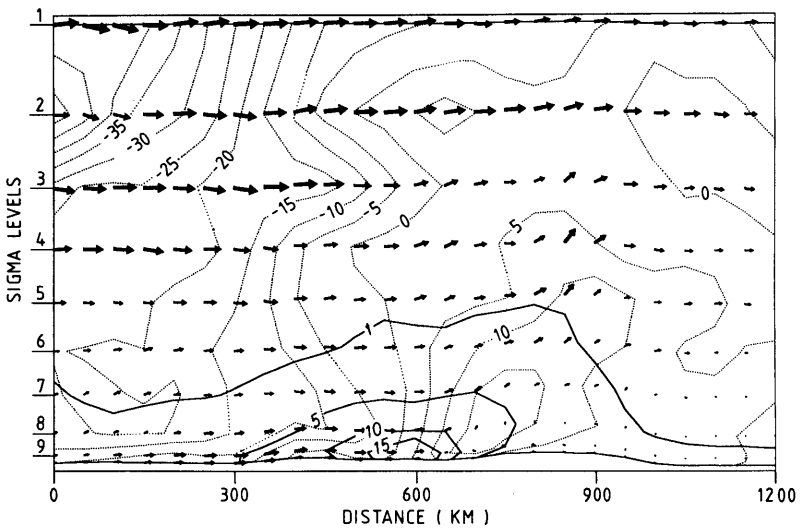

Fig. 6. Vertical cross-section (A to B in Fig. 5) of normal wind (m s^{-1}) (dotted lines), S–SO_2(a) (μg-sulfur/kg-air) (solid lines) and tangential- and vertical wind (arrows) after 18 h integration. An arrow of horizontal length of about 50 km corresponds to 40 m s^{-1} of horizontal wind. A vertical arrow of the distance between consecutive sigma-levels corresponds to approximately 3 Pa s^{-1}.

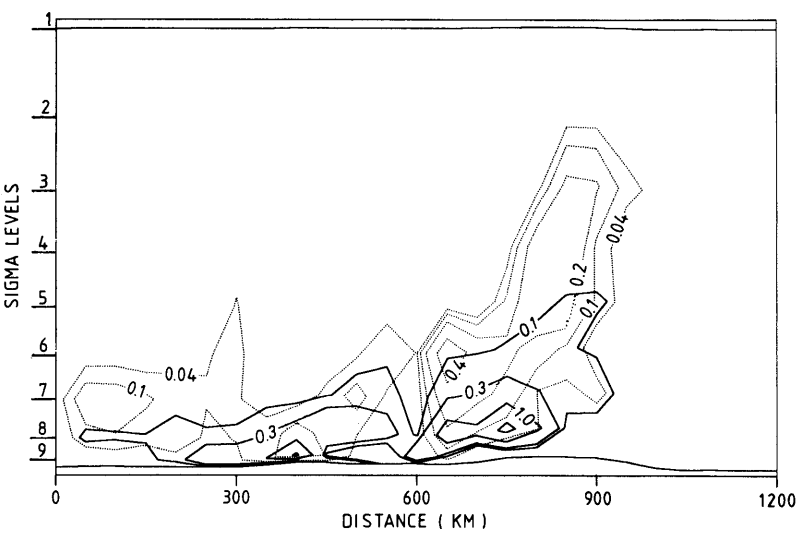

Fig. 7. Vertical cross-section (A to B in Fig. 5) of cloud water content (g-water/kg-air) (shaded areas) and S–SO_4(a) (μg-sulfur/kg-air) (solid lines) after 18 h integration.

existed over the main emission areas in Europe, while at the end a cold and convectively unstable air mass with showers, penetrated into northwest Europe. In Figs. 6 and 7, vertical cross-sections of modelled fields perpendicular to the occluded warm front at 18 h are shown. Upward motions associated with the front give S–SO_2(a) values of about 1 μg-sulfur/kg-air up to σ-level 5 (Fig. 6). Strong north- and westward transport of S–SO_2(a) takes place parallel to and ahead of the

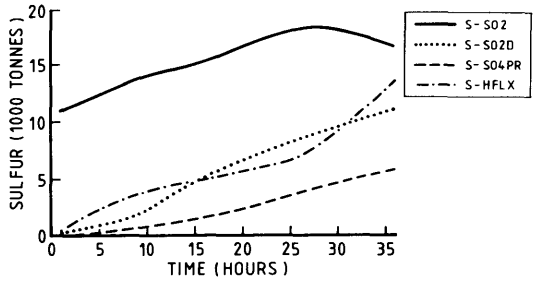

Fig. 8. Sulfur budget quantities for the 36-h simulation period given as total amount of S–SO_2 in the model domain, accumulated dry deposition (S–SO_2 D), accumulated wet deposition (S–SO_4 PR) and accumulated horizontal flux out through the boundaries (S-HFLX). The accumulated quantities are equal to zero initially.

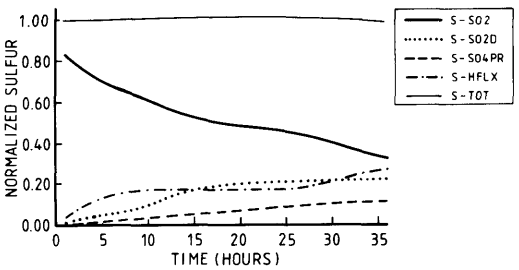

Fig. 9. The same quantities as in Fig. 8 and in addition sulfur in all modelled variables (including deposition and flux through the boundaries), divided by the sum of the total initial mass and total accumulated emission.

front in the lowest model layers (Fig. 6). In Fig. 7 the clouds associated with the warm front and the showers behind the front are clearly seen. The maximum liquid water content of about 0.4 g-water/kg-air is found at σ-level 6 approximately above the occlusion at the surface. The S–SO_4(cl) has a maximum of about 2 μg/sulfur/kg-air in the lower parts of the clouds.

5.2. *Initial fields*

The initial conditions are obtained by running the model for the preceding 24 h, starting from zero concentrations. From experiments with the present synoptic situation (not shown), we can infer a spin-up time for integrated S–SO_2(a) and S–SO_4(a) of 20–30 h. Thus, it has been assumed that a 24 h simulation is needed to give the initial fields. The in-cloud S–SO_4(cl) field starts from zero. The spin-up time for the clouds is estimated to average 6–8 h and to be greater for high-level clouds than low-level clouds (Sundqvist et al., 1989).

5.3. *The sulfur budget*

Fig. 8 shows different sulfur quantities integrated over the whole model domain. We see that the total S–SO_2(a) content increases during the first 25–30 hours, while it decreases in connection with the strong outflow across the boundaries during the last hours. The accumulated dry deposition is about 40% higher than the wet deposition. Fig. 9 shows the same budget quantities and the accumulated sulfur mass in all components (S-TOT, including loss by advection through the boundaries), divided by the sum of accumulated emissions and the initial sulfur mass. A S-TOT line equal to 1 represents a perfect mass balance, provided that there is no change in the integrated air mass. We see that the model is satisfactorily mass conserving. Furthermore, the figure shows that the simulation is initialized with a partitioning between S–SO_2(a) and S–SO_4(a) of about 5–6/1. After 36 h, about 32% is left in the form S–SO_2(a), about 61% has either been transported out through the boundaries or deposited at the ground, and about 7% remains on the components S–SO_4(a) and S–SO_4(cl).

During the 36-h simulation period, 22% of the emitted sulfur has been added to the initial mass (not shown). The partitioning of the remainder is 17% on wet deposition, 27% on dry deposition and 34% on transport out through the horizontal boundaries.

5.4. *Comparison with surface measurements*

First, it must be emphasized that a good quantitative agreement between the model simulations and observations cannot be expected, especially due to the simple treatment of the sulfur chemistry, the emission fields and the advection term. However, a qualitative agreement may be expected so a comparison can help to indicate shortcomings of the model.

24-h mean surface measurements of S–SO_2(a), S–SO_4(a) and S–SO_4(pr) (sulfate in precipitation) available from the EMEP-measuring network in

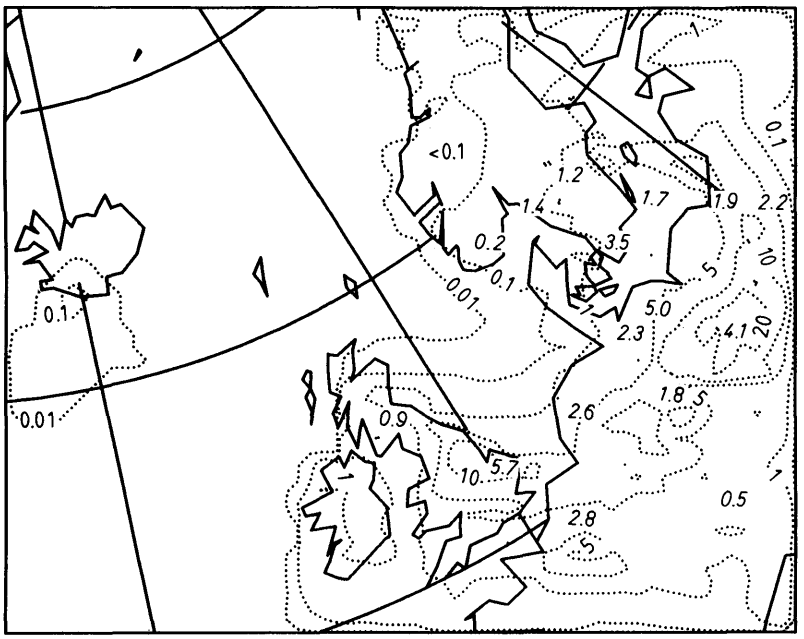

Fig. 10. Simulated S–SO_2 field (dotted lines for 0.01, 0.1, 1, 5, 10 and 20 $\mu g/m^3$) at σ-level 10 after 30 h of integration, valid time 006*Z* 6 September 1985. The surface measurements are mean values for the period 006*Z* 5 September to 006*Z* 6 September 1985.

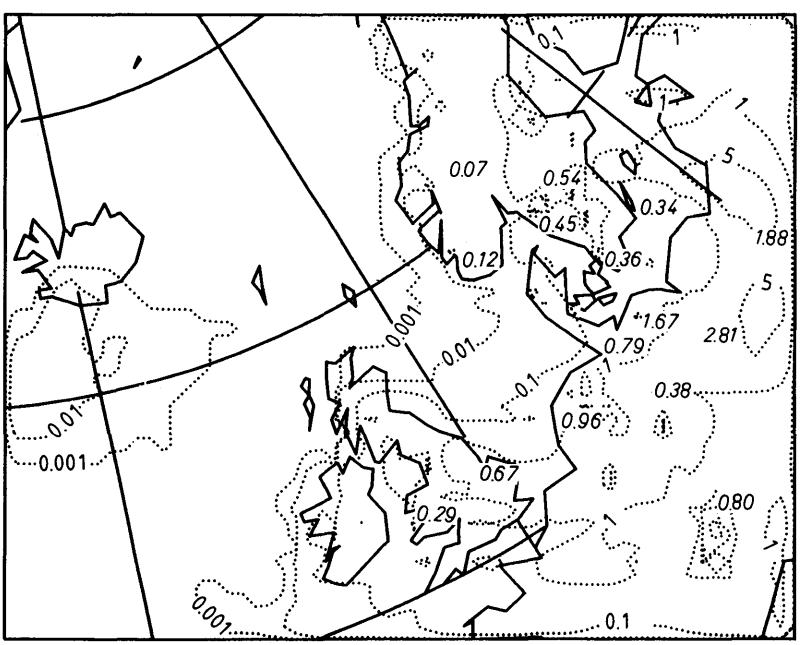

Fig. 11. As Fig. 10, but for S–SO_4 in air.

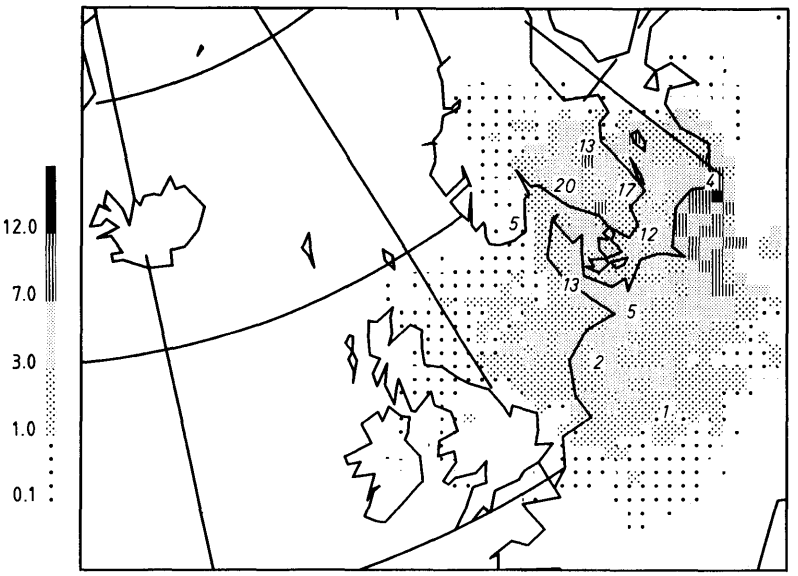

Fig. 12. Simulated 24-h accumulated wet deposition of sulfate in rain (kg km^{-2}) between 6 h and 30 h of simulation time. The surface measurements (small numbers) are accumulated values for the same time period.

Europe (Pacyna et al., 1987), are given together with model simulations in Fig. 10, 11 and 12. Even though the measurements are sparse in parts of the model domain, it seems that the model overestimates the S–SO_2(a) concentration in the source region, while the estimates are more realistic over Scandinavia. Some of the discrepancy in central Europe might be because the EMEP-stations are situated in background areas, while the model gives a mean for both background and source areas. Furthermore, the measurements are close to the surface while the model values are a mean between the ground and 80 m. Thus in both cases the model values should be somewhat higher than the measurements.

An overestimation of S–SO_2(a) close to the sources indicate that the transport away from the source region is inefficient. This emphasizes the importance of vertical transport. Enhanced vertical transport will reduce the concentrations at low level close to the source. In addition the choice of emission level, chemical transformation rates and dry deposition will affect the low level SO_2-concentration. This problem is further discussed in the next section.

For S–SO_4(a) too low values are obtained over Scandinavia, while more realistic values are obtained in the source areas. The modelled accumulated wet deposition is mainly in the range 3–10 kg km^{-2} day^{-1} in southern Scandinavia, while twice this amount is observed (10–20 kg km^{-2} day^{-1}). In Poland the model estimates are up to 10–15 kg km^{-2} day^{-1}, but there are no measurements to verify them. In central Europe, the model estimates are closer to the observed values.

A comparison of the simulated initial fields at 00Z, 5 September 1985, with measurements also indicate an overestimation of the S–SO_2(a) close to the sources, and an underestimation of S–SO_4(a) over Scandinavia.

A simple test is performed to check whether the underestimation of sulfate in air and precipitation in Scandinavia might be explained by the lack of background fields. The level 10 background values are simply put equal to 0.1 μg/kg-air and 0.2 μg/kg-air for S–SO_2(a) and S–SO_4(a) respectively, which closely corresponds to the background values applied in the planetary boundary layer in the EMEP-model (Eliassen et al., 1988). At higher model levels, the mixing ratios are put equal to the level 10 value multiplied with the σ-value at the level in question. The wet deposition pattern including

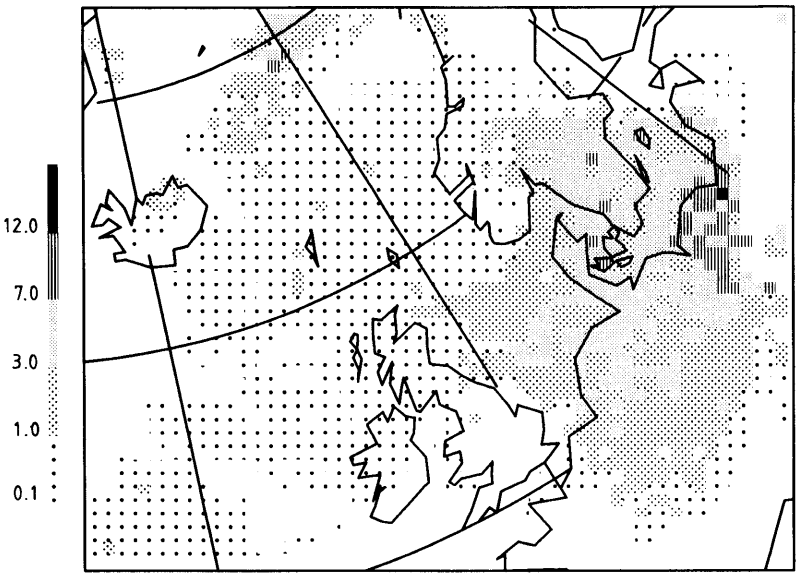

Fig. 13. As Fig. 12, but with background concentrations of S–SO_2 and S–SO_4 in air.

the background fields, is shown in Fig. 13. Only a slight increase in the deposition is observed over southern Scandinavia. The S–SO_4(a) field is also still underestimated in Scandinavia (not shown). Thus it is not likely that the observed discrepancies can be explained only by the lack of background sulfur. Results from this test is also shown in Table 1.

One other possible error source is the fact that the boundary values are put equal to zero. However, since the transport near the sources during this simulation (see Figs. 2 and 5) is mainly outwards across the boundaries, the addition of boundary values has little effect.

The above results suggest that the transformation from S–SO_2(a) to S–SO_4(a) given by k_1 in (3.5), is too slow. k_1 will primarily depend on the amount of the main sulfur oxidizing species OH, O_3 and H_2O_2, which may vary considerably in both space and time during a 36 h simulation. An increase in k_1 would in the present case, make the simulations compare better with the observations. However, such experiments become quite meaningless since k_1 depends on unknown parameters as OH, O_3 and H_2O_2. Instead a more realistic experimentation with sulfur transformations can be employed, when the model includes gas and liquid phase chemistry explicitly.

Furthermore, since the near source values of SO_4(a) agree quite well with observations, it is not likely that the 10% of the emission considered as SO_4(a) should be increased.

One should also mention that the underestimated sulfate deposition partly might be due to the neglected sub-cloud scavenging, specially close to the sources where the sub-cloud concentrations are high.

At the station in southeast Norway, the model yields almost no deposition, while about 5 kg km^{-2} day^{-1} is observed. This is mainly due to an error in the simulated precipitation field, which was shifted southeastward compared to the observations (Sundqvist et al., 1989). This shift might be due to a shift in the circulation pattern around the low. Thus some of the discrepancies in the simulated sulfur fields are also connected to errors in the AMUB-model.

5.5. *Sensitivity tests*

In Table 1, the sensitivity of some important sulfur quantities to the variations of model parameters, is shown.

The antidiffusion technique has been applied to all three sulfur compounds and the cloud water. In Fig. 14 we see that, compared to the reference run in Fig. 10, a reduction in the

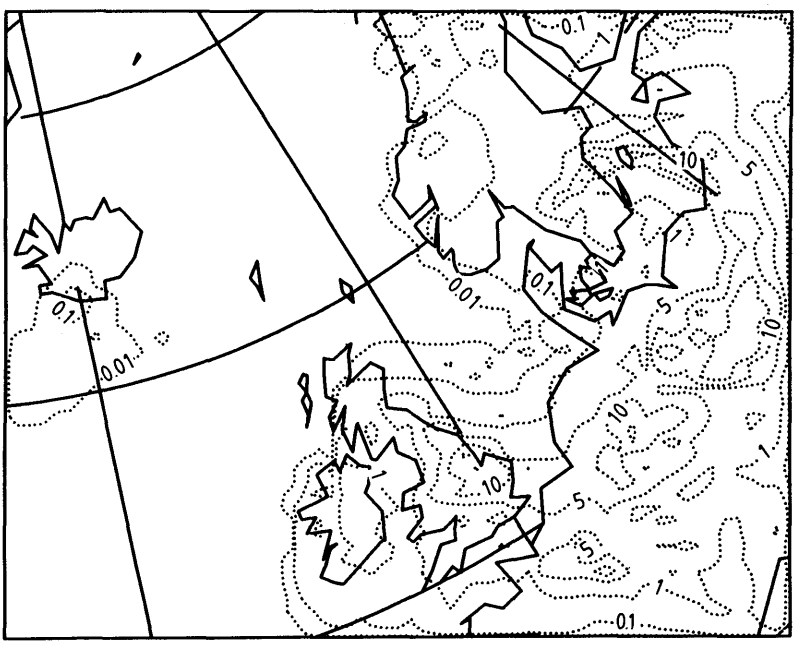

Fig. 14. As Fig. 10, but with the shape preserving antidiffusion technique applied to the advection of the sulfur quantities and cloud water.

Table 1. *Sensitivity to the tests (1)–(5) of 30 h accumulated dry deposition (D-DEP), wet deposition (W-DEP) and horizontal flux through the boundaries (H-FLUX), and the mean and maximum σ_{10} level values of S–SO_2(a) and S–SO_4(a) at +30 h*

	Accumulated until +30 h			At +30 h			
	D-DEP	W-DEP	H-FLUX	$\overline{S\text{–}SO_2}$	$\overline{S\text{–}SO_4}$	$(S\text{–}SO_2)_{max}$	$(S\text{–}SO_4)_{max}$
Ref.	1	1	1	1	1	1	1
(1)	1	0.96	1	1	1.08	1.24	1.18
(2)	0.63	1.08	1.05	1.35	1.16	1	1
(3)	0.94	1.01	1.01	1.02	1.01	1.02	1
(4)	0.86	0.94	1.08	1.18	1.29	0.78	0.69
(5)	0.84	1.04	1.10	0.85	0.84	0.76	0.79
(6)	1	1.67	1.37	0.96	1.13	1	1
Ref.	8.6	4.9	8.7	1.36	0.38	54.2	11.4
	(10^3 tonnes-S)			(μg-S/kg-air)			

The table numbers are fractions of the reference values. In the last row the absolute values of the reference run are given.

Ref. Reference run corresponds to the presented model formulation.

(1) The upstream advection scheme is replaced by the shape preserving antidiffusion scheme.

(2) The dry deposition velocities are reduced to the half.

(3) The dry deposition is replaced by an alternative formulation (see Subsection 3.2).

(4) The eddy diffusion is replaced by an alternative parameterization (see Subsection 5.4).

(5) 30% of the level 9 emission is released in level 8.

(6) Background fields according to Subsection 5.3 are added to the reference run.

$S–SO_2(a)$ values in the North Sea, and higher values close to the warm front over the Baltics are found. This indicates that the shape of the sulfur fields is now better preserved. The total wet deposition is reduced by 4% (Table 1). Still, a slight increase in the wet deposition over southern Scandinavia is found, which also suggests that the pollutants now are more concentrated. But, compared to the run with the upstream scheme the differences are quite small. This is because of the poor resolution of the emission field which means that the $S–SO_2(a)$ and $S–SO_4(a)$ fields are smoothed out from the beginning. Thus since the gradients are weak a diffuse scheme will perform almost as well as a shape preserving advection technique. A better effect of the shape preserving technique is expected when a higher resolution of the source field is obtainable.

Applying the antidiffusion technique is computationally expensive. For the present simulation, about 30% more CPU-time was needed.

Test 2 in Table 1 shows a model run where the dry deposition velocities are reduced by 50%. The total dry deposition is then 37% lower, while the wet deposition only increases by 8%. Moreover, the mean value of $S–SO_2(a)$ increases substantially. This demonstrates that the dry deposition affects the ground air concentration substantially, while wet deposition of sulfate is less sensitive. In test 3 Isaksen and Rodhe (1978) formulation of the dry deposition is applied (see Subsection 3.2). It reduces the total dry deposition with about 6%. The effect on the other quantities is small.

To illustrate the importance of the vertical diffusion (test 4 in Table 1) we perform a model run with a different parameterization scheme given by Pleune (1989). This scheme tries to include the vertical transport by so called intermittent turbulence in a stable atmosphere, which so far has been strongly underestimated in numerical models (Mahrt, 1987). The basic assumption of this scheme is (1) that the vertical eddy transport is confined to a certain number of subgrid scale patches with concentrated windshear and temperature gradients, and (2) that the Richardson number equals the critical Richardson number in each patch. The net effect is to enhance vertical exchange in stable layers compared to the AMUB-model. Substantial effect on all parameters in Table 1 is found. Again the total wet deposition is the least sensitive parameter. We also observe that the mean concentrations have increased as a result of increased downward transport from the emission level 9 to the surface layer 10. Of special interest is the lowering of the surface maximum concentrations in the source area. This indicates an improvement in the calculated $S–SO_2(a)$, and demonstrates the importance of the formulation of the vertical exchange.

In test 5, a model run with 30% emission into level 8 and 70% into level 9, is shown. The effects are much the same as in test 4. However, the mean ground concentrations are now reduced compared to the reference run.

6. Summary and conclusions

A regional Eulerian 3-D numerical sulfur transport model has been developed and tested. The model is developed from a NWP-model with a refined treatment of condensation and cloud formation, and explicit calculation of cloudwater. It has 10 layers in the vertical and 50 km horizontal resolution.

A main aim with this study has been to couple a regional sulfur transport model to a meteorological model, with emphasis on including the wet scavenging of sulfur into a realistic description of clouds and precipitation. Emphasis is also put on a numerical formulation which is mass conserving, positive definite and suitable as a basis for further model development.

36-h simulations are made for one synoptic situation, and the shortcomings of both the sulfur parameterization and the NWP-model are analysed by looking at numerical diffusion, dry- and wet deposition, vertical transport and emission distribution, and the chemical transformation rate.

Budget estimates show that the model is satisfactorily mass conserving. The sensitivity tests indicate that the wet deposition is much more dependent on the oxidation rate than on other processes. Comparisons with surface measurements of sulfate in air and precipitation show a good qualitative agreement. But, too low sulfate amounts in both rainwater and air are found in

areas with substantial transport of sulfur with anthropogenic origin. One important reason for this is probably that the employed bulk transformation rate from SO_2 to sulfate in air to is too slow. However, a realistic experimentation with the transformation rates requires inclusion of explicit treatment of gas and liquid phase chemistry, which has been omitted in this study. Further investigations are initiated on this problem.

Furthermore, the low level concentrations of sulfur dioxide are also qualitatively realistic, but close to the sources they are overestimated. The simulations indicate that this is partly due to underestimation of the vertical transport in the lowest model layers. The chemical transformation rates, the dry deposition and the choice of emission heights also affect the low level concentrations.

The poor resolution of the emission field strongly smooths out the sulfur dioxide and sulfate fields in air. And since the gradients in these fields therefore become weak, the effect of applying an antidiffusion advection scheme is small compared to the more diffusive normal upstream scheme. Still, a slight improvement of the simulation of sulfur compounds in both dry air and precipitation is indicated.

The model presented has proven to be a basis for further research. In addition to the above mentioned inclusion of gas and cloud phase chemistry, it would be meaningful with investigations of sensitivity to vertical transport, shape preserving advection routines, parameters of the condensation scheme, vertical distribution and horizontal resolution of the emission field.

7. Acknowledgements

I wish to thank Professor H. Sundqvist for many valuable discussions and suggestions during this study. I also thank Professor H. Rodhe and Mr. I. Dugstad for contributing to improve this work, and Mr. J. Saltbones and Dr. S. Grønås for putting the emission field and the meteorological data at my disposal. The work was supported by a grant D.41.12.029 from the Norwegian Research Council, and it was performed under a joint research project with Bergen Scientific Centre (BSC). All the simulations were performed on the IBM 3090/200VF at BSC.

8. Appendix

Scale analysis of the flux divergence formulation of the advection equation

The flux divergence form of the advection equation from eq. (3.1) is (assuming $m = 1$):

$$\frac{\partial \psi}{\partial t} = -\nabla_H \cdot (\boldsymbol{V}_H \psi) - \frac{\partial}{\partial \sigma}(\dot{\sigma}\psi) - \frac{\psi}{p^*}\left(\frac{\partial p^*}{\partial t} + \boldsymbol{V}_H \cdot \nabla_H p^*\right). \quad \text{(A1)}$$

We now apply a scale analysis to eq. (A1) to investigate the magnitude of the three different terms on the right-hand side. The scales of the weather system applied to the SULFUR-model (see Fig. 5) are similar to the scales used in Holton (1979) (pp. 26–53). Following Holton's analysis and assuming that the horizontal and the vertical concentration fluctuation scale, $\Delta\psi/\psi$, is approximately 1 we get

$V_H \approx 10$ m s^{-1}	horizontal velocity scale
$\dot{\sigma} \approx 10^{-6}$ s^{-1}	vertical velocity scale (≈ 1 cm s^{-1})
$L \approx 10^6$ m	length scale
$\sigma \approx 1$	depth scale ($\approx 10^4$ m)
$T \approx 10^5$ s	time scale
$\Delta p/p^* \approx 10^{-2}$	horizontal pressure fluctuation scale
$\Delta\psi/\psi \approx 1$	horizontal and vertical concentration fluctuation scale

Applying the above scales to eq. (A1) yields:

$$\nabla_H \cdot (\boldsymbol{V}_H \psi) \approx \psi\ 10^{-5}\ \text{s}^{-1},$$

$$\frac{\partial}{\partial \sigma}(\dot{\sigma}\psi) \approx \psi\ 10^{-6}\ \text{s}^{-1},$$

$$\frac{\psi}{p^*}\left(\frac{\partial p^*}{\partial t} + \boldsymbol{V}_H \cdot \nabla_H p^*\right) \approx \psi\ 10^{-7}\ \text{s}^{-1}.$$

From this scale analysis it is seen that, on an average, it is reasonable to neglect the last term in eq. (A1).

REFERENCES

Berge, E. 1988. An examination of three numerical schemes for solving the advection equation. IBM Bergen Scientific Centre, Bergen, Norway. *IBM report nr. 88/38*, 20 pp.

Brost, R. A., Haagenson, P. L. and Kuo, Y. H. 1988. The effect of diffusion on tracer puffs simulated by a regional scale eulerian model. *J. Geophys. Res. 93, No. D3*, 2389–2404.

Chang, J. S., Brost, R. A., Isaksen, I. S. A., Madronich, S., Middleton, P., Stockwell, W. R. and Walcek, C. J. 1987. A three-dimensional eulerian acid deposition model: Physical concepts and formulation. *J. Geophys. Res. 92, No. D12*, 14681–14700.

Charmichael, G. R. and Peters, L. K. 1984a. An eulerian transport/transformation/removal model for SO_2 and sulfate. 1. Model development. *Atmos. Environ. 18*, 937–951.

Charmichael, G. R. and Peters, L. K. 1984b. An eulerian transport/transformation/removal model for SO_2 and sulfate. 2. Model calculation of SO_x transport in the eastern united states. *Atmos. Environ. 18*, 953–967.

Charmichael, G. R., Peters, L. K. and Kitada, T. 1986. A second generation model for regional-scale transport/chemistry/deposition. *Atmos. Environ. 20*, 173–188.

Chaumerliac, N., Nickerson, E. C. and Rosset, R. 1987. Sulfur scavenging in a mesoscale meteorological model with semispectral microphysics. *J. Geophys. Res. 92, No. D3*, 3114–3126.

Eliassen, A., Hov, Ø., Iversen, T., Saltbones, J. and Simpson, D. 1988. Estimates of airborne transboundary transport of sulphur and nitrogen over Europe. *The Norwegian Met. Inst. EMEP/MSC-W report 1/88*, Oslo, Norway, 79 pp.

Eliassen, A. and Saltbones, J. 1983. Modelling of long-range transport of sulfur over Europe: A two year model run and some model experiments. *Atmos. Environ. 17*, 1457–1473.

Fowler, D. 1980. Removal of sulfur and nitrogen compounds from the atmosphere in rain and by dry deposition. *Proc. Int. Conf. Ecol. Impact Acid Precip.*, 22–31, SNSF-project, Ås-NLH, Norway, 22–32.

Grønås, S., Foss, A. and Lystad, M. 1987. Numerical simulations of polar lows in the Norwegian Sea. *Tellus 39A*, 334–353.

Holton, J. R. 1979. An introduction to dynamic meteorology. *New York, Academic Press*, 391 pp.

Hov, Ø., Eliassen, A. and Simpson, D. 1988. *Calculation of the distribution of the NO_x compounds in Europe. Tropospheric Ozone* (ed. I. S. A. Isaksen). Dordrecht, Reidel, 239–261.

Isaksen, I. and Rodhe, H. 1978. A two-dimensional model for the global distribution of gases and aerosol particles in the troposphere. Univ. of Stockholm, Dept. of Met., *Report AC-47*, 36 pp.

Karamchandani, P. and Peters, L. K. 1983. Analysis of the error associated with grid representation of point sources. *Atmos. Environ. 17*, 927–933.

Kristjansson, J. E. 1990. Model simulations of an explosive meso β-scale cyclone: The role of condensation parameterization. *Tellus 42A*, 78–91.

Mahrt, L. 1987. Grid averaged surface fluxes. *Mon. Wea. Rev. 115*, 1550–1560.

McRae, G. J., Goodin, W. R. and Seinfeld, J. H. 1982. Numerical solution of the atmospheric diffusion equation for chemically reacting flows. *J. Comp. Phys. 45*, 1–42.

McRae, G. J., Goodin, W. R. and Seinfeld, J. H. 1982. Development of a second-generation mathematical model for urban air pollution. 1. Model formulation. *Atmos. Environ. 16*, 679–696.

Mesinger, F. and Arakawa, A. 1976. Numerical methods used in atmospheric models, volume I. *GARP Publications Series No. 17*, WMO/ICSU, 64 pp.

Middleton, P., Chang, J. S., Del Corral, J. C., Geiss, H. and Rosinski, J. M. 1988. Comparison of RADM and OSCAR precipitation chemistry data. *Atmos. Environ. 22*, 1195–1208.

Nordeng, T. E. 1987. The effect of vertical and slantwise convection on the simulation of polar lows. *Tellus 39A*, 354–375.

Nordlund, G. 1986. Local deposition of sulfur: A comparison of Finnish estimates and EMEP model (EMEP-west) values. In *Atmospheric computations to assess acidification in Europe: work in progress* (ed. J. Alcamo and J. Bartnicki). IIASA, Laxenburg, Austria, RR-86-5, 27–29.

Pacyna, J., Schaug, J., Harstad, A., Krognes, T. and Skjelmoen, J. E. 1987. *Data report July–December 1985, EMEP/CCC-report 6/87*. The Norwegian Institute for Air Research, Lillestrøm, Norway, 233 pp.

Pleune, R. 1989. A parameterization of the vertical eddy diffusion in stable situations and its impact on a numerical acid rain prediction model. Univ. of Bergen, Sec. of Met., *Report no. 3-1989*, 50 pp.

Prahm, L. P., Conradsen, K. and Nielsen, L. B. 1980. Regional source quantification model for sulfur oxides in Europe. *Atmos. Environ. 14*, 1027–1054.

Pudykiewicz, J., Benoit, R. and Staniforth, A. 1985. Preliminary results from a partial LTRAP model based on an existing meteorological forecast model. *Atmos. Oce. 23*, 267–303.

Richtmyer, D. and Morton, K. W. 1967. *Difference methods for initial-value problems*. 2nd edition. Wiley. New York, 405 pp.

Rodhe, H., Crutzen, P. and Vanderpool, A. 1981. Formation of sulfuric and nitric acids in the atmosphere during long-range transport. *Tellus 33*, 132–141.

Rodhe, H. and Grant, L. 1983. Summer and winter budgets for sulfur over Europe. *Idöjaras 87*, 1–6.

Rood, R. B. 1987. Numerical advection algorithms and their role in atmospheric transport and chemistry models. *Rev. Geophys. 25*, 71–100.

Rutledge, S. A., Hegg, D. A. and Hobbs, P. V. 1986. A numerical model for sulfur and nitrogen scavenging in narrow cold-frontal rainbands. 1. Model description and discussion of microphysical fields. *J. Geophys. Res. 91*, 14385–14402.

Sehmel, G. A. 1980. Particle and gas dry deposition: A review. *Atmos. Environ. 14*, 983–1011.

Seinfeld, J. H. 1975. *Air pollution: physical and chemical fundamentals*. McGraw-Hill, 506–514.

Seinfeld, J. H. 1986. *Atmospheric chemistry and physics of air pollution*. Wiley, New York, 738 pp.

Smolarkiewicz, P. K. 1983. A simple positive definite advection scheme with small implicit diffusion. *Mon. Wea. Rev. 111*, 479–486.

Smolarkiewicz, P. K. 1984. A fully multidimensional positive definite advection transport algorithm with small implicit diffusion. *J. Comp. Phys. 54*, 325–362.

Sundqvist, H., Berge, E. and Kristjansson, J. E. 1989. Condensation and cloud parameterization studies with a mesoscale NWP model. *Mon. Wea. Rev. 117*, 1641–1657.

Tremblay, A. and Leighton, H. 1985. A three-dimensional cloud chemistry model. *J. Cli. Appl. Met. 25*, 652–671.